

Performance Enhancement of a Low-Pressure Ratio Centrifugal Compressor Stage with a Rotating Vaneless Diffuser by Impeller Disk Extended Shrouds

S. Seralathan[†] and D. G. Roy Chowdhury

Hindustan Institute of Technology and Science, Padur, Tamilnadu, 603 103, India

[†]Corresponding Author Email: siva.seralathan@gmail.com

(Received May 5, 2015; accepted January 6, 2016)

ABSTRACT

Numerical simulations have been carried out to examine the performance and flow parameters of forced rotating vaneless diffuser obtained by the extension of impeller disks of a low-pressure ratio shrouded type centrifugal compressor stage with diffuser diameter ratio 1.40. Four different levels of shroud extensions (i.e., impeller disks alone) forming the rotating vaneless diffusers are analyzed at four different flow coefficients. The extension of impeller disks alone by 40% of impeller exit diameter leads to a fully forced rotating vaneless diffuser thereby replacing the existing stationary vaneless diffuser. The comparative studies are performed using the same impeller with a stationary vaneless diffuser also having a diffuser diameter ratio of 1.40. Static pressure rise in ES40 is found to be higher than SVD by around 9.84% at design flow coefficient and also at above off-design flow rates. Energy coefficient is highest for ES40, followed by ES30 compared to SVD. For ES40, the static pressure recovery coefficient also is higher compared to SVD. The efficiency of ES40 is lesser by around 5.40% to 3.43% compared to SVD, at design as well as at above off-design flow coefficients. The stagnation pressure losses for ES40 drastically reduced compared to SVD. The comparison of stagnation pressure contours and absolute velocity contours near the hub and shroud walls of ES40 and SVD configurations shows that the rotating diffuser walls as in ES40 causes further addition of energy to the fluid. This adds up the kinetic energy level of the fluid which due to better diffusion, results in gain of static pressure rise. Moreover, there is a net increase in stagnation pressure distribution at the exit of diffuser due to rotating vaneless diffuser. Also, the presence of a fully rotating vaneless diffuser (ES40) smooth out the distorted entry flow profiles, thereby improving the performance of the centrifugal compressor stage.

Keywords: Centrifugal compressor; Shrouded impeller; Shroud extend; Forced rotating vaneless diffuser; Stationary vaneless diffuser.

NOMENCLATURE

C	absolute velocity	Φ	flow coefficient
C_m	meridional velocity	ψ_{loss}	stagnation pressure loss coefficient
C_p	static pressure coefficient	ψ_p	static pressure recovery coefficient
C_{po}	total pressure coefficient	ψ	energy coefficient
C_u	tangential velocity	η	efficiency
N	rotational speed	ρ	air density
P	static pressure	1	impeller inlet
P_o	stagnation pressure	2	impeller exit
r	radius	2'	impeller blade exit
R	radius ratio	2''	impeller disks exit
U	impeller tip speed	3	stationary vaneless diffuser inlet
W	specific work	3'	rotating vaneless diffuser inlet
X	span normalized	3''	rotating vaneless diffuser exit
		4	stationary vaneless diffuser exit

SVD	stationary vaneless diffuser	ES30	extended shrouds by 30%
ES10	extended shrouds by 10%	ES40	extended shrouds by 40%
ES20	extended shrouds by 20%		

1. BACKGROUND AND OBJECTIVE

The flow leaving the rotating impeller is very complex and non-uniform in both axial (i.e., hub-to-shroud) and circumferential (i.e., blade-to-blade) directions. This non-uniform flow then enters the diffuser and its behavior in the diffuser has determining effect on the centrifugal compressor performance. The stage performance of the centrifugal compressor depends upon the interaction of flow between the upstream component, impeller and downstream component, the diffuser and its impact on performance of both the individual components. Numerous investigations on the flow through the centrifugal impeller were performed by researchers. The studies have established the presence of separated zones (i.e., jet and wake regions) at the impeller exit region, which reduces the expected pressure rise in the impeller passage. An effective pressure recovery system downstream of an impeller is very important to achieve high efficiency and high pressure ratio. Hence, selection of an appropriate diffuser is a critical step to achieve this. The development of newer non-conventional diffuser design is necessary in reducing the losses in energy level related due to diffusion.

Rotating the vaneless diffuser is one such non-conventional diffuser design evolved in overcoming the deficiencies of pressure rise in conventional radial diffuser. The concept of rotating vaneless diffuser with forward curved rotor blade and radial tipped rotor blade has stirred the imagination of centrifugal compressor and pump designers (Novak 1907; Erwin *et al.* 1969) due to the significant performance improvements. Rotating vaneless diffuser is broadly categorized as free rotating vaneless diffuser and forced rotating vaneless diffuser. In the forced rotating vaneless diffuser, the diffuser part is combined with the rotating impeller and its rotational speed is equal to that of the impeller. This is created by two types of design concepts i.e., shroud extension and blade cutback. In the shroud extension concept, the rotating vaneless diffuser is formed by the extension of impeller's disks alone beyond the blade tip. In this paper, the numerical investigations of forced rotating vaneless diffuser based on the shroud extension design concept are discussed.

Earlier, Sapiro (1983) carried out experimental investigations on a low-pressure ratio centrifugal compressor having backward swept impellers with vaneless diffusers of diffuser diameter ratio 1.5776. The forced rotating vaneless diffuser was formed by the extension of shrouds up to 20 percent beyond the diameter of impeller blade.

The results from tests indicated that the use of impeller-extended shrouds marginally improved the efficiency of centrifugal compressor with high-specific speed stages. Similarly, tests by Northern Research and Engineering Corporation (1976) showed that the performance only deteriorated for shroud extension beyond 25 percent of the backward swept impeller blade diameter. Recently, Govardhan *et al.* (2011) and Seralathan *et al.* (2013) conducted preliminary numerical investigations on forced rotating vaneless diffuser with a radial tipped centrifugal impeller compressor stage. Also, Seralathan *et al.* (2014) performed studies on a backward curved impeller with extension of impeller disks by 40% beyond the diameter of impeller blade tip. The results showed that the rise in static pressure improved with lesser stagnation pressure losses. The concept of extending the shrouds (i.e., impeller disks) have been very widely accepted in the compressor industry for low-pressure ratio centrifugal compressors, with a reported gain of 1-2 % in stage efficiency (Govardhan *et al.* 1978; James M Sorokes 2011; Chen Xu *et al.* 2012). However, the limits to shroud extensions were never reported. Systematic study of flow behavior inside the forced rotating vaneless diffuser based on shroud extension concept is not available in the open source. No literature is available in the open source focusing on completely replacing the existing stationary vaneless diffuser with a forced rotating vaneless diffuser of equivalent diffuser diameter ratio. Also, numerical analysis involving rotating vaneless diffuser concept, is also limited to a very few (Aboujaib *et al.* 1998). Recently, Yasutoshi Senoo (2005) highlighted about the improved efficiency of centrifugal impeller by the industrial practices of extending only the diameter of both the disc and shroud ring of the rotating impeller.

A shrouded type centrifugal impeller with a diffuser diameter ratio 1.40 is chosen for the present study. The present studies are focused to numerically investigate the effect of forced rotating vaneless diffuser formed by shroud extension concept on a low-pressure ratio centrifugal compressor. Various flow parameters and performance characteristics are studied in detail to understand the flow mechanism involving this concept in a better manner. In this present study, impeller disks alone (i.e., hub and shroud portion of the shrouded type impeller) are extended by 10, 20, 30 and 40% above the diameter at exit of impeller and the performance of such configurations are compared with the same shrouded type centrifugal impeller with a stationary vaneless diffuser in the downstream having a diffuser diameter ratio 1.40.

Table 1 Dimensional details of the shrouded type centrifugal impeller (Govardhan *et al.* 1978)

Diameter at exit of the impeller	D ₂	570 mm	Thickness of the blade	T	6 mm
Diameter at inlet of the impeller	D ₁	215.2 mm	Width of blade at inlet	b ₁	58.5 mm
Outer diameter to inner diameter ratio	D ₂ /D ₁	2.649	Width of blade at exit	b ₂	27.6 mm
Diameter at exit of the impeller disk	D ₂ '	570 mm	Blade angle at the inlet	β ₁	44.6°
Diameter at exit of the impeller blade	D ₂ '	570 mm	Blade angle at the exit	β ₂	90°
Rotational speed of the impeller	N	1500 rpm	Number of blades	Z	18

Table 2 Geometric dimensional details – impeller with extended shroud forming rotating vaneless diffuser and conventional stationary vaneless diffuser

Configurations		Stationary vaneless diffuser		Rotating vaneless diffuser	
		Diffuser inlet diameter (D ₃)	Diffuser outlet diameter (D ₄)	Diffuser inlet diameter (D ₃ ')	Diffuser outlet diameter (D ₃ '')
Conventional impeller with stationary vaneless diffuser (SVD)		570 mm	798 mm	---	---
Extended Shroud Configurations	Impeller with 10% extended shroud with respect to D ₂ ' (ES10)	627 mm	798 mm	570 mm	627 mm
	Impeller with 20% extended shroud with respect to D ₂ ' (ES20)	684 mm	798 mm	570 mm	684 mm
	Impeller with 30% extended shroud with respect to D ₂ ' (ES30)	741 mm	798 mm	570 mm	741 mm
	Impeller with 40% extended shroud with respect to D ₂ ' (or) Impeller with forced rotating vaneless diffuser (ES40)	---	---	570 mm	798 mm
Diffuser diameter ratio D ₄ /D ₃ (or) D ₃ '/D ₃ '		1.40		1.40	

2. DETAILS OF THE CENTRIFUGAL COMPRESSOR

For the present numerical investigations, a low-pressure ratio centrifugal compressor is chosen. Table 1 shows the specification of the compressor. A centrifugal impeller (Govardhan *et al.* 1978) with diffuser diameter ratio (D₄/D₃) of 1.40 is chosen for the present study. The centrifugal impeller with a stationary vaneless diffuser (SVD) having a diffuser diameter ratio of 1.40 is modeled. This is used as the basis for comparing the performance of the stage. The impeller with extended shroud (ES10) is created by extending the impeller disks alone by 10% of its diameter at exit of the impeller (D₂') without affecting the blade tip geometry. Similarly, ES20, ES30 and ES40 are created by extending the impeller disks alone by 20%, 30% and 40% of its diameter at exit of the impeller (D₂').

By increasing the impeller disks alone gradually from 10 to 40% of impeller exit diameter (D₂'), the extended impeller disks effectively replaces the stationary vaneless diffuser at 40% of impeller exit diameter, as the diffuser diameter ratio is 1.40 in the present study. Thus, the extension of impeller disks alone by 40% of impeller exit diameter creates a fully forced rotating vaneless diffuser. The dimensional details of the forced rotating vaneless

diffuser and stationary vaneless diffuser are given in Table 2. The study is conducted at design flow coefficient, Φ = 0.27 and also at three above off-design flow coefficients namely, Φ = 0.30, Φ = 0.34 and Φ = 0.37.

3. COMPUTATIONAL METHODOLOGY

The modeling of the computational domain as well as meshing is done by using ANSYS ICEM CFD 13.0. Figure 1 shows the computational domains of various configurations. The computational domain models deployed for the numerical simulations of flow through centrifugal compressor stage of ES10, ES20, ES30, ES40 and SVD configurations consists of an impeller blade and vaneless diffuser. Based on the assumption that flows are periodic in each impeller blade passages, one blade passage (i.e., single passage approach) is configured in this present analysis. The passage considered here is half the blade spacing on either sides of the blade. This approach helps in avoiding the need to model the complete centrifugal compressor impeller domain, thereby reduces the computational resource requirements and time. The entire computational domain is meshed by generating a grid with unstructured tetrahedral elements having prism layers in the near-wall regions. Prism layer cells are introduced around the impeller blade, near the hub

and shroud wall of both the impeller and diffuser to enable the cells to be positioned nearer to the boundary. A minimum of seven prism layers is introduced in the near wall regions as seen in the Fig. 2. A minimum y^+ value of 0.10 and a maximum y^+ value of 1.0 are maintained for generated mesh in the near-wall regions according to the turbulence modeling requirements. Table 3 shows the grid independency study for SVD. With reference to grid G1, the percentage difference for grid G2 is less and grid G2 is taken up for the present studies. Similar analysis are performed for other configurations but not shown here. Based on the grid independence study, the overall quantity of tetrahedral as well as prism elements sum up to 899833 and 902111 elements for the configuration of SVD as well as ES10 and 903137, 855483 and 899833 elements for ES20, ES30 and ES40 configurations respectively.

Table 3 Grid independency study for SVD

Grid (G)	Nodes	Elements	C_p	Difference in %
G1	335304	1042798	0.849	---
G2	240442	899833	0.843	0.706%
G3	173866	572403	0.831	2.120%

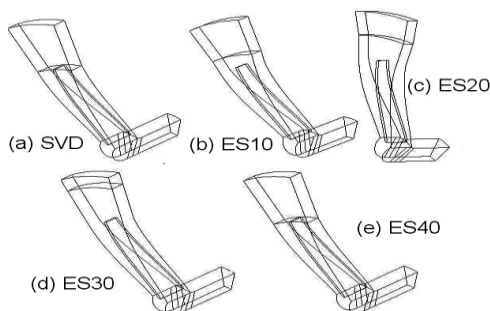


Fig. 1. Computational geometry of (a) SVD, (b) ES10, (c) ES20, (d) ES30 and (e) ES40.

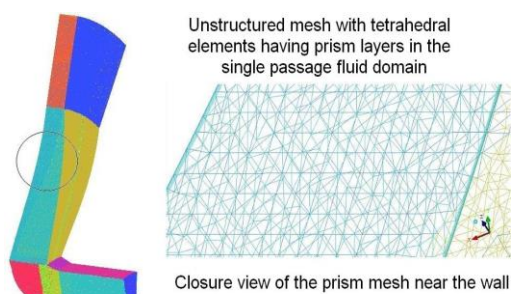


Fig. 2. Computational domain with tetrahedral elements having prism layers in the near wall regions.

The boundary conditions enforced at each boundaries of the fluid domain in the present studies are shown in Fig. 3 and Fig. 4. Inlet boundary of the fluid domain is shifted ahead by half of the impeller blade chord length from the eye of the impeller. This is done to make sure that the

boundary condition at inlet is not influenced by the back pressure of the impeller blade. The whole computational domain is modeled in rotating frame of reference. At inlet, the total pressure in stationary frame is specified as the boundary condition for the fluid domain. Specification of uniform inflow direction normal to the inlet plane is quite justified as the boundary at the inlet is shifted ahead from the impeller blade. The reference pressure mentioned for the present simulations are 101.325 kPa. Therefore, at inlet the relative total pressure is zero Pascal. Air at 25°C is the fluid specified for the present studies. The turbulence model imposed for the studies is standard $k-\omega$ (Wilcox) and turbulence intensity of 5% is specified at the inlet. Rotational periodic boundary conditions are imposed at either side wall of the computational domain. At outlet, mass flow rate is specified for the passage which takes into account the number of the impeller blades in the computational domain. The blade, hub and shroud of the impeller as well as the rotating vaneless diffuser and stationary vaneless diffuser are imposed with wall boundary conditions and rotating with same angular velocity equivalent to the computational domain. Therefore, it is stationary relative to the rotating frame of reference. The stationary domain (i.e., stationary vaneless diffuser) is enforced with counter-rotating type boundary condition for the reason that diffuser walls do not rotate in a stationary frame of reference.

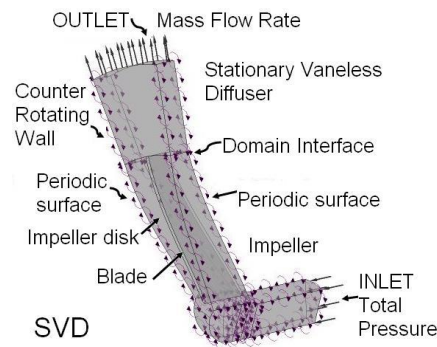


Fig. 3. Boundary conditions for the centrifugal impeller with stationary vaneless diffuser.

As the computational domain have both rotating domain (i.e., impeller and forced rotating vaneless diffuser created by extended shroud concept) as well as stationary domain (i.e., stationary vaneless diffuser), appropriate interfaces are to be introduced connecting the rotating domain and stationary domain which links the meshes together across the frame change. In this present studies involving steady-state simulations, frozen rotor is selected for the rotor-stator frame change interface. This is a robust model and utilizes lesser computer resource compared to other interface models. The walls are imposed with no slip condition. The wall roughnesses are ignored by considering it as smooth walls. The numerical simulations are done by using

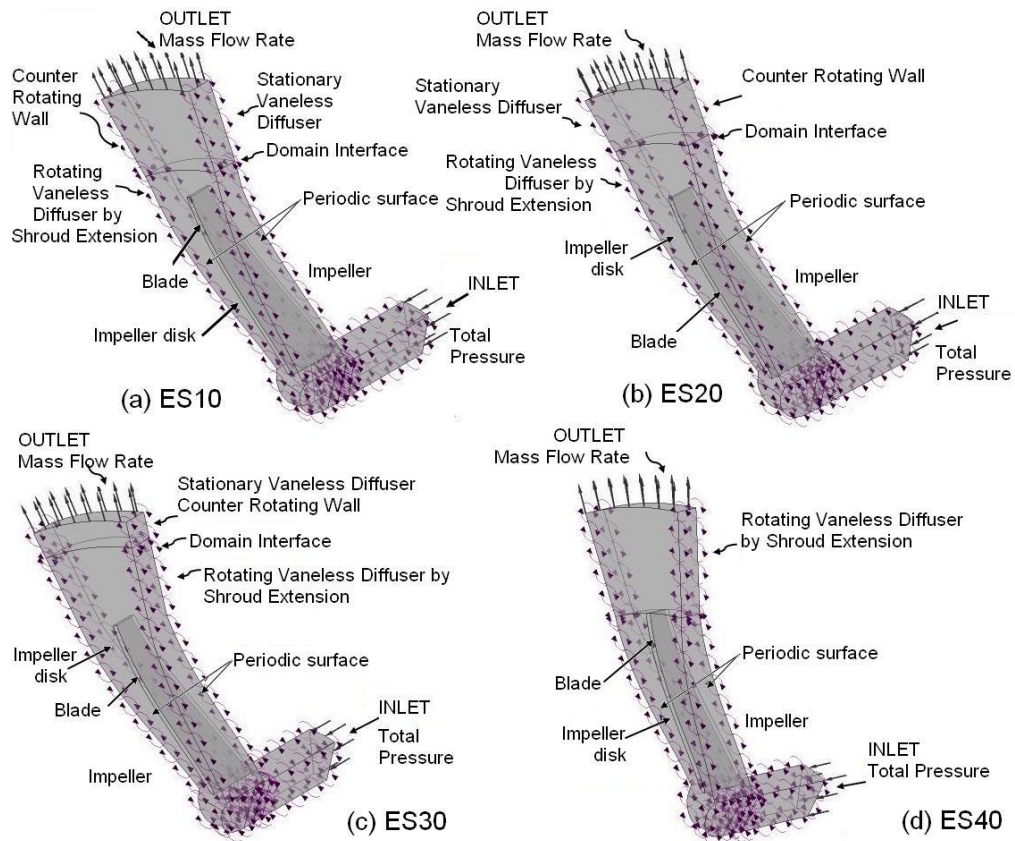


Fig. 4. Boundary conditions for the centrifugal impeller with rotating vaneless diffuser by various extended shroud configurations.

commercial CFD code based on the finite volume numerical method - ANSYS CFX 13.0 to solve the full three dimensional Reynolds Averaged Navier Stokes Equations. Automatic timestep are used for all the governing equations with timestep values equal to $0.2/\omega$, where ω is defined as the angular velocity in rad/sec. The computations of the steady-state solutions are carried out till the residual values are converged. CFX uses coupled solver and the normalized residuals in general is given by

$$\left[\frac{\square}{r_\phi} \right] = \frac{[r_\phi]}{a_p \Delta \phi}$$

where r_ϕ is the raw residual control volume imbalance, a_p is representative of control volume coefficient and $\Delta \phi$ is a representative range of the variable in domain. For the present computations involving all the governing equations, the convergence criteria of RMS (root mean square) normalized values of the equation residuals are set to 1×10^{-4} .

4. VALIDATION

The geometric details of the low-pressure ratio centrifugal impeller selected for the present investigations are given in Table 1 (Govardhan *et al.* 1978). The numerical results based on standard $k-\omega$ (Wilcox) as well as $k-\omega$ based Shear Stress Transport (SST Mentor) turbulence models carried out under steady-state conditions are compared with the available experimental results done by

Govardhan *et al.* (1978). Figure 5 shows the comparison of experimental and numerical data obtained at exit of a radial tipped impeller alone between its hub and shroud for dimensionless static pressure coefficient. It is observed (as seen in Fig. 5) that values obtained with standard $k-\omega$ turbulence model are closer to the data measured under experimental conditions. Therefore, subsequent numerical studies are carried out by using standard $k-\omega$ (Wilcox) turbulence model.

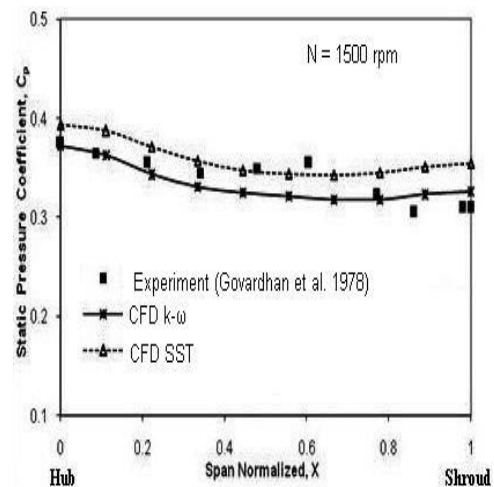


Fig. 5. Comparison of C_p at exit of a radial tipped centrifugal impeller with various turbulence models.

5. RESULTS AND DISCUSSION

5.1 Performance of the Compressor Stage

The performance characteristics of the centrifugal compressor with ES10, ES20, ES30, ES40 and SVD configurations at the design speed of 1500 rpm for efficiency and stage energy coefficient against flow coefficient are shown in Fig. 6(a) and Fig. 6(b) respectively. It is seen from the Fig. 6(a) that efficiency is highest for ES10, 3.40% higher than that of SVD, followed by ES20. The efficiency of ES30 is almost similar to that of SVD, whereas for ES40, the efficiency is lesser than SVD by around 4.5%. It is also observed that in all the configurations for the present studies, as the mass flow rate increases the efficiency decreases. The rotating vaneless diffuser created by the extension of impeller disks alone results in higher disk friction losses. The disk friction is a parasitic loss that further adds to the exit total temperature of the fluid at compressor stage exit. As ES40 has the highest component of rotating vaneless diffusers, the isentropic efficiency of ES40 is therefore found to be the least for the entire flow range due to the increase in actual total temperature at stage exit. This drop in efficiency is the outcome of increased stagnation pressure distribution (as seen in Fig. 14(c) which is discussed later) obtained with the centrifugal compressor stage having a fully rotating vaneless diffuser (ES40).

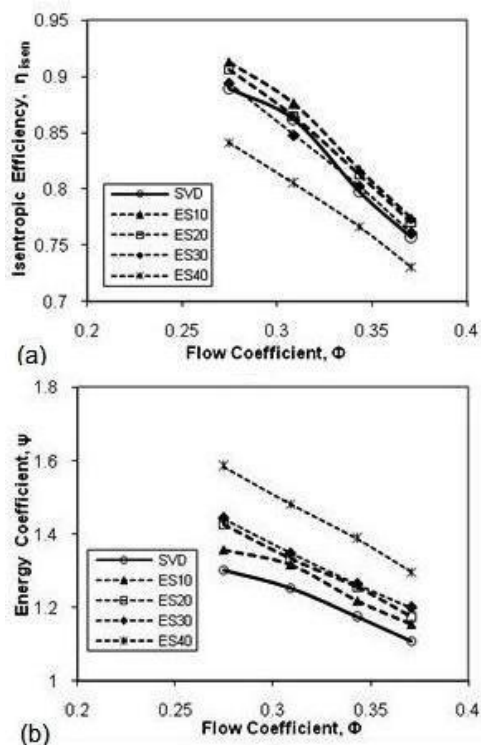


Fig. 6. (a) Variation of isentropic efficiency with flow coefficient and (b) Variation of energy coefficient with flow coefficient.

Figure 6(b) shows the distribution of stage energy coefficients against flow coefficients. The energy coefficient data indicates the quantity of energy

obtained by the fluid, as the fluid go through the centrifugal compressor stage comprising impeller and diffuser. The choking limit and its highest value of the energy coefficient decide the stable operating range of the compressor. The energy coefficient, ψ , is highest for ES40, 21% higher compared to SVD, followed by ES30 by 10.7%, and then by ES20 and ES10. The energy coefficient values of SVD are the lowest. Energy coefficient is a measure of rise in pressure in the centrifugal compressor and at design point the energy coefficient is more in the case of ES40 compared to SVD.

5.2 Diffuser Performance

The diffuser performances are estimated by the physical flow properties determined at the diffuser domain's inlet and outlet. The diffuser performances are evaluated by stagnation pressure loss coefficient, ψ_{loss} and static pressure recovery coefficient, ψ_p . Static pressure recovery coefficient indicates the extent to which the static pressure is recovered from the available total energy at the inlet of diffuser.

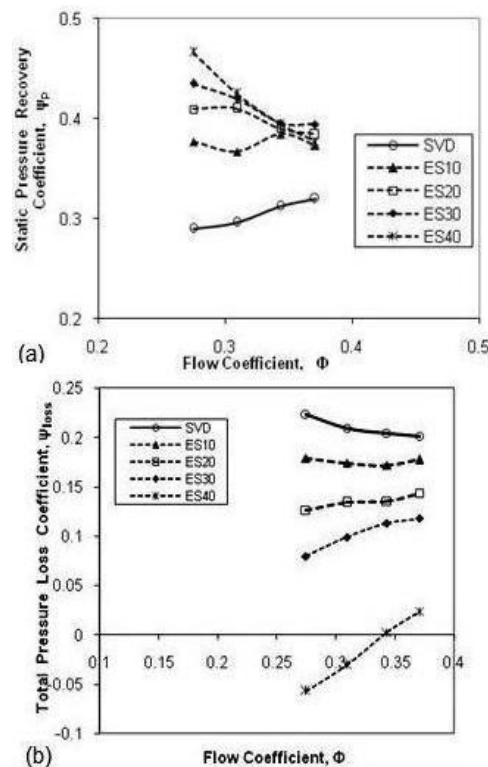


Fig. 7. (a) Static pressure recovery coefficient with flow coefficient and (b) Stagnation pressure loss coefficient with flow coefficient.

The variation of static pressure recovery coefficient with flow coefficient is shown in Fig. 7(a). As the mass flow rate increases, the static pressure recovery coefficient also increases for SVD. For ES10 and ES20, the values of static pressure recovery coefficient remain almost constant throughout the entire range of flow coefficient, whereas for ES30 and ES40 configurations, the static pressure recovery decreases for increase in

flow rate. At design flow condition, the static pressure recovery for ES40 is highest followed by ES30. Static pressure recovery of SVD is the lowest compared to all other configurations. Since the static pressure recovery coefficients of the entire variations of extended shrouds are higher than SVD, the static pressure rise obtained is also higher for extended shroud configurations. This indicates that diffusion process is better in rotating vaneless diffuser based on shroud extend concept compared to SVD.

The variation of stagnation pressure loss coefficient with flow coefficient is shown in Fig. 7(b). The increase in values of stagnation pressure loss coefficient shows the extent to which the losses occur within the flow passage due to friction and mixing of fluids with different energy levels. The stagnation pressure loss coefficient for SVD decreases slightly with the increase in flow coefficient, whereas for ES10, the losses remains almost constant up to flow coefficient, $\Phi = 0.34$ and increases slightly afterwards. For ES20, ES30 and ES40, the stagnation pressure loss coefficients are lowest at design flow coefficient and increases with the increase in flow coefficient.

In conventional SVD, the shear loss caused by the flow is due to its logarithmic path length and dynamic head which depend on the absolute velocity i.e., its direction and magnitude of the flow at exit of the impeller. But, in a rotating vaneless diffuser, the losses caused by the flow due to its path length and dynamic head are based on the relative velocity i.e., its direction and magnitude of the flow in the diffuser. The magnitude of relative velocity is smaller and to a large extent radially directed compared to absolute velocity. The relative flow angle is also higher than the absolute flow angle. Therefore, losses due to friction are lesser in the rotating vaneless diffuser compared to conventional stationary vaneless diffuser. The losses in the shroud extend configurations are lesser due to the presence of rotating diffuser walls, which reduces the shear between the through flow and walls compared to SVD. The formation of boundary layer in a rotating part of the vaneless diffuser is lesser compared to stationary vaneless diffuser. This helps in improving the performance of the compressor for ES10, ES20 and ES30 as seen in Fig. 6(a) and Fig. 6(b). This is not the case for ES40, as the actual total temperature of the fluid at compressor stage exit is added up due to disk friction. As the rotating vaneless diffuser portion is higher compared to other shroud extend configurations (ES10, ES20 and ES30), ES40 configuration has the lowest stagnation pressure loss coefficient.

As seen in Fig. 7(b), the stagnation pressure loss coefficient values are negative for design flow condition $\Phi = 0.27$ and above off-design flow coefficient $\Phi = 0.30$ for fully rotating vaneless diffuser configuration (ES40). This indicates a net gain of the stagnation pressure loss coefficients at these flow conditions. This is due to additional energy added to the fluid by the rotating part of the vaneless diffuser. The net gain in energy is realized by overcoming the total pressure losses that occur

due to friction within the passage. At $\Phi = 0.34$, the loss in total pressure is balanced by the energy gain realized due to rotating vaneless diffuser and the value of stagnation pressure loss coefficient is nearly zero. The fully rotating vaneless diffuser shows a net gain in total pressure initially and then losses occur as the flow rate is increased. The stagnation pressure loss coefficient for other shroud extension configurations are much lesser compared to SVD. This clearly reveals that there is a net gain in energy level in the fluid for centrifugal compressor stage with rotating vaneless diffuser, which results in a net gain in stagnation pressure distribution.

This is primarily due to the energy gain achieved by the fluid as a result of the rotating part of the vaneless diffuser formed by the extension of impeller disks alone by overcoming / reducing the losses due to friction. From these present numerical studies involving various shroud extension configurations, it is clear that by keeping the rotational speed of the diffuser walls equivalent to that of impeller, the stagnation pressure losses can be substantially reduced leading to better compressor stage performance and diffuser performance. Also, the rotating vaneless diffuser results in raising the kinetic energy of the fluid which converts into additional static pressure rise due to better diffusion process (as seen in Fig. 17 which is discussed later) for fully rotating vaneless diffuser configuration (ES40) compared to stationary vaneless diffuser.

5.3 Flow Parameters

The velocity vectors on span-wise surface for conventional stationary vaneless diffuser (SVD) and fully rotating vaneless diffuser (ES40) from hub to shroud closer to the hub wall ($x/b = 0.10$), mid span location ($x/b = 0.50$) as well as closer to the shroud wall ($x/b = 0.90$) for the design flow coefficient, $\Phi = 0.27$ are shown in Fig. 8(a) and Fig. 8(b) respectively. From the vector plots of SVD and ES40, the fluid of low kinetic energy region (wake) and fluid of high kinetic energy region (jet) are clearly visible. As seen in Fig. 8(a) for SVD, the mixing of fluid with different energy levels takes place inside the diffuser region and proceeds in the radial direction of stationary vaneless diffuser. At exit of the diffuser, the flow is observed to be slightly uniform in nature, whereas it is found to be highly non-uniform at the impeller exit region and at entry region of the diffuser. For a fully rotating vaneless diffuser (ES40) as seen in Fig. 8(b), the flow is observed to be highly non-uniform at the impeller exit region and at entry region of the rotating vaneless diffuser. The double swirl is observed immediately at the entry region of the rotating vaneless diffuser. The mixing of fluid with different energy levels is delayed and it takes place later in the rotating vaneless diffuser.

The mixing of fluid with different energy levels results in significant loss of dynamic component of the stagnation pressure along with a rise in static pressure due to diffusion process. This has a significant bearing on the conversion into static pressure rise by diffusion. Also, the losses due to

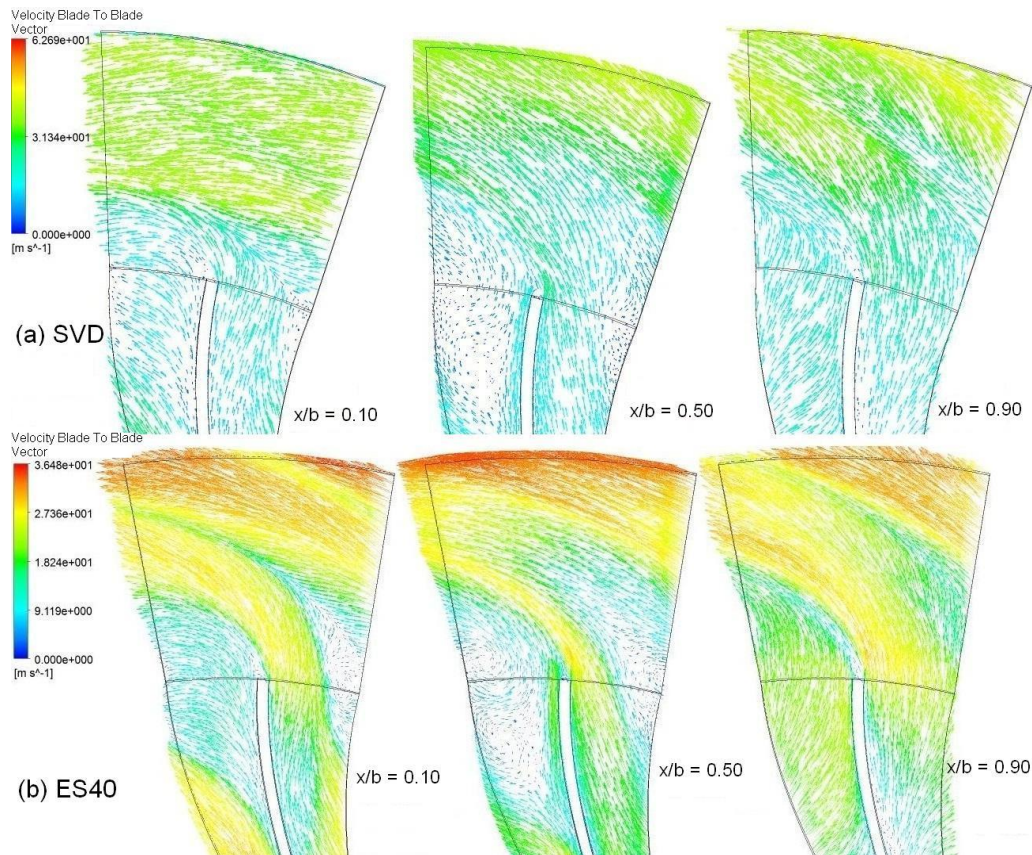


Fig. 8. Velocity vector plot across the span from hub to shroud at design flow coefficient.

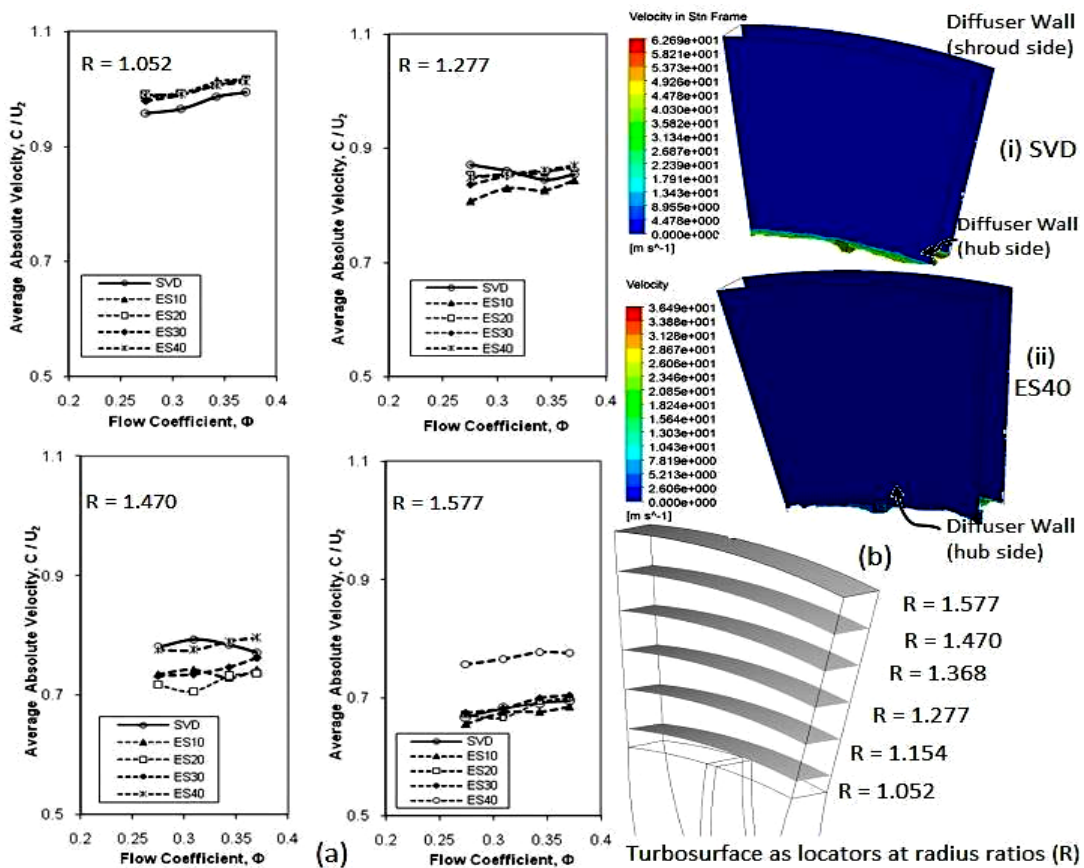


Fig. 9. (a) Variation of mass averaged non-dimensional absolute velocity with flow coefficient for various configurations (b) Velocity observed at diffuser walls for SVD and ES40.

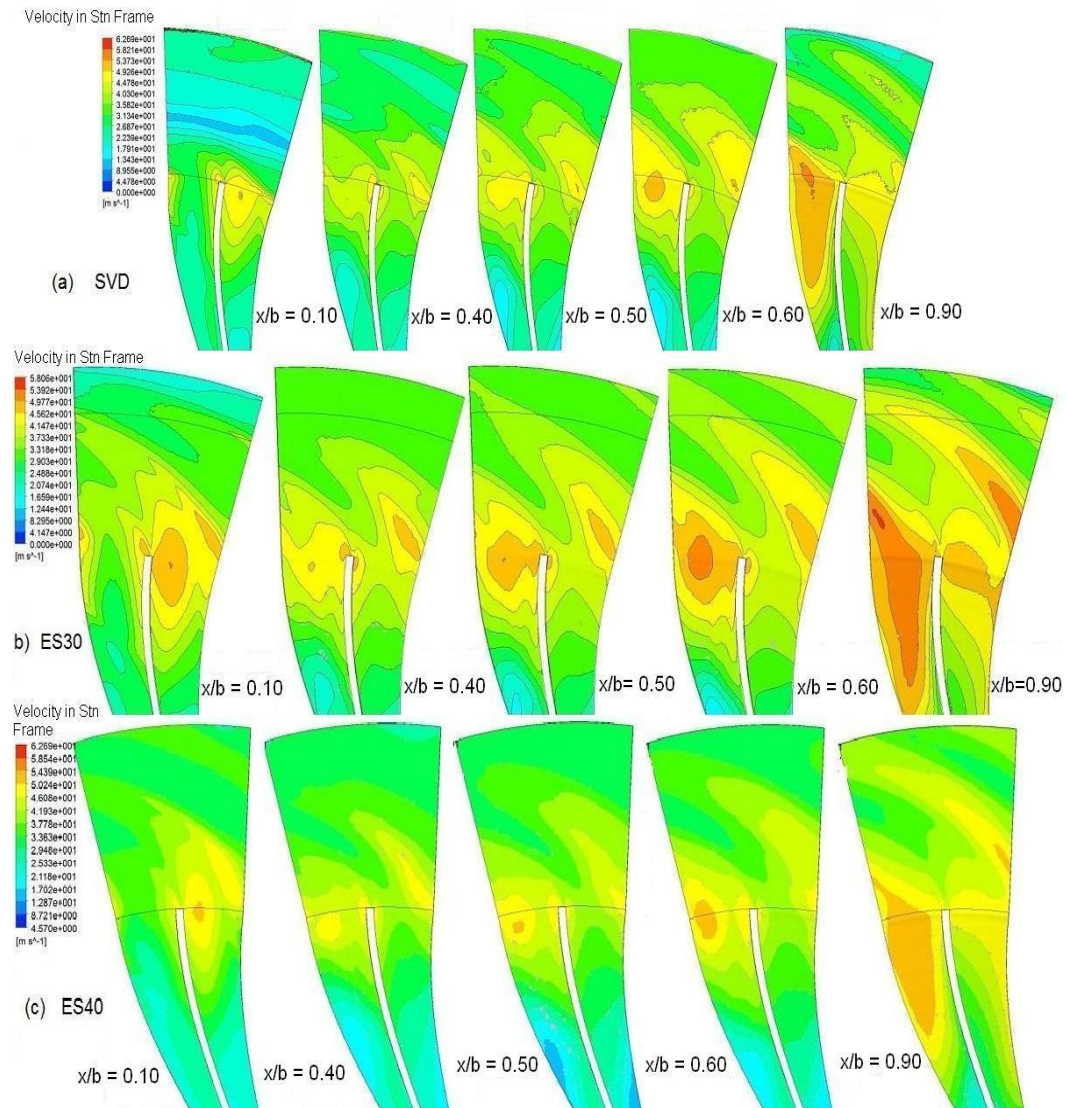


Fig. 10. Contours of absolute velocity distribution on the axial plane at $x/b = 0.10, 0.40, 0.50, 0.60$ and 0.90 for design flow coefficient, $\Phi = 0.27$ for (a) SVD (b) ES30 and (c) ES40 configuration.

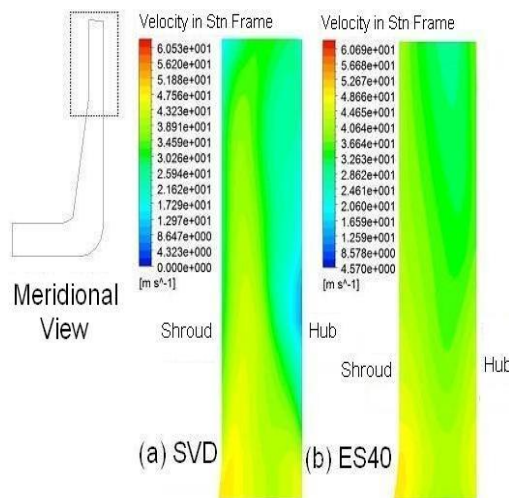


Fig. 11. Meridional view plots of absolute velocity distribution for ES40 and SVD at design flow coefficient, $\Phi = 0.27$.

mixing are an important source of inefficiency. From the vectors plots, it is clear that the losses due to mixing are considerably reduced with fully rotating vaneless diffuser created by extended shroud concept. The stagnation pressure loss coefficient for ES40 is the least followed by ES30 (as seen in Fig. 7(b)), which is much lesser than that of SVD by 125% to 88% at design and off-design flow coefficients. This reveals that the losses due to mixing are considerably reduced with extended shroud configuration. The mass averaged absolute velocity distribution across the width from exit of the impeller to the exit of the diffuser at different radial locations with various flow coefficients is presented in Fig. 9(a). In general, the absolute velocity increases with flow coefficient for all the configurations. However, at diffuser inlet ($R = 1.052$), the absolute velocities of all the shroud extend configurations are above SVD. As the radius ratio increases and the diffusion occur within the flow passage, absolute velocity decreases for all the

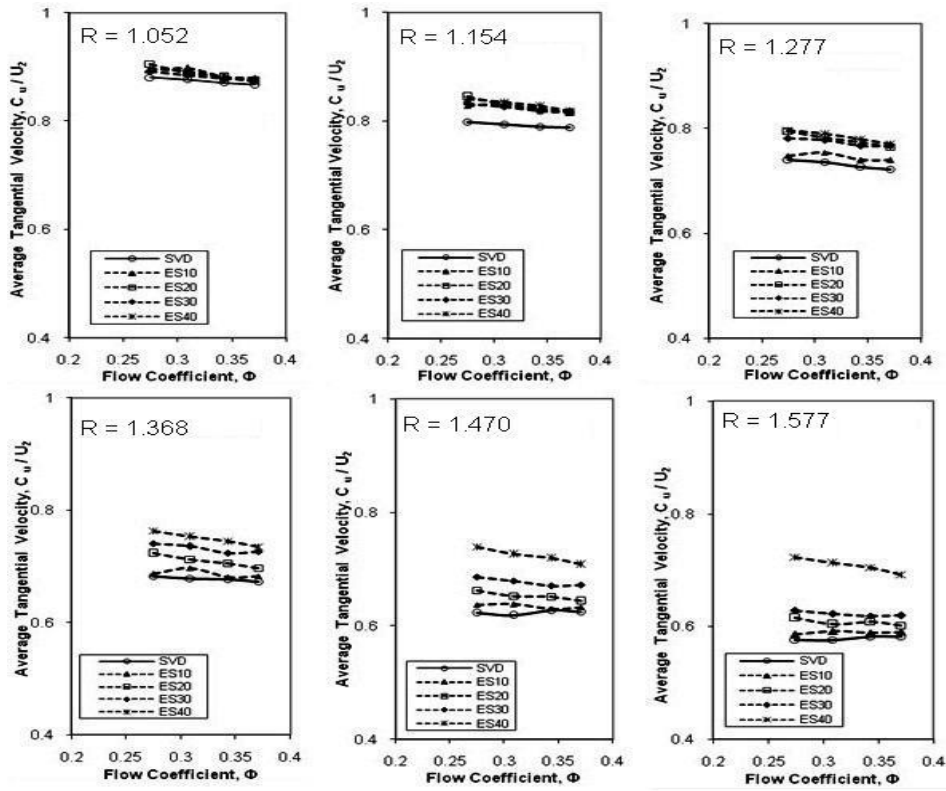


Fig. 12. Variation of mass averaged tangential velocity with flow coefficient for various configurations.

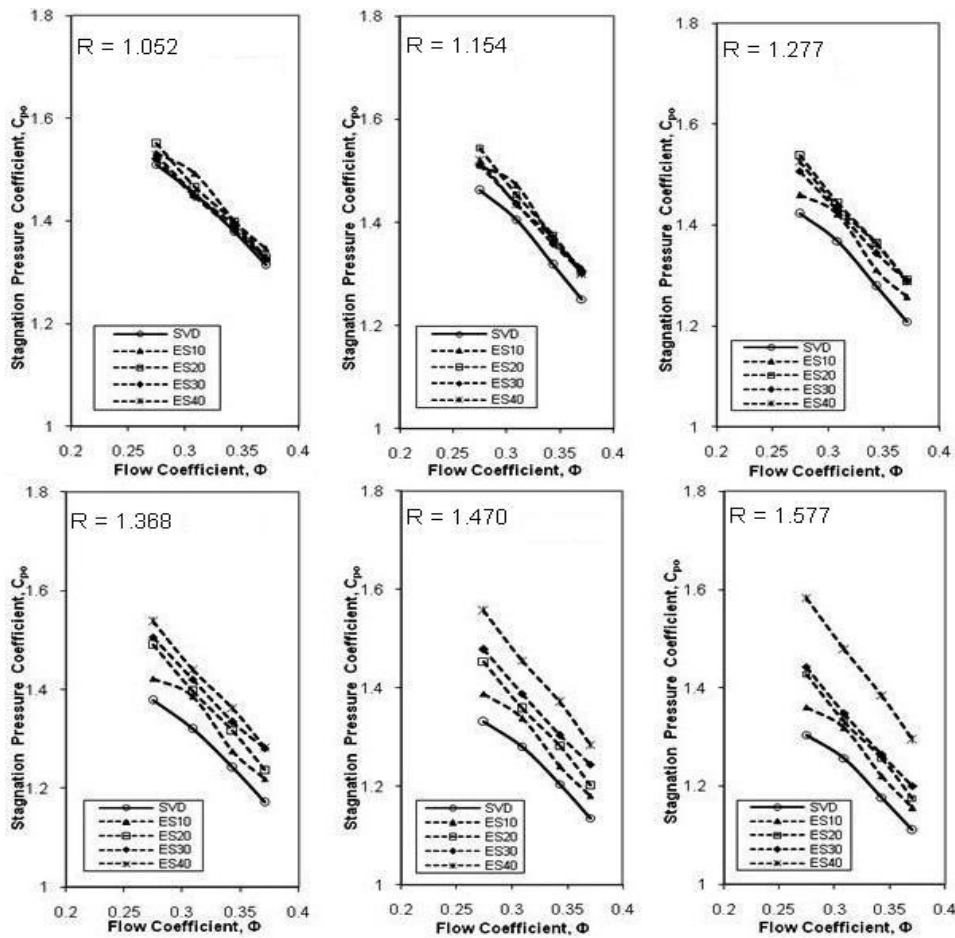


Fig. 13. Variation of stagnation pressure coefficient with flow coefficient for various configurations.

configurations. The absolute velocity difference between the inlet and outlet of the diffuser indicates the amount of kinetic energy transformation which is reflected as static pressure rise. This is not strictly true if work input (i.e., addition of energy level to the fluid) is added by causing the walls of the vaneless diffuser component to rotate at a speed equivalent to the impeller rotational speed as in the present simulation studies. Figure 10(a), 10(b) and 10(c) shows the absolute velocity contours on the axial plane from hub to shroud for design flow coefficient, $\Phi = 0.27$. By comparing the absolute velocity contours closer to the hub wall ($x/b = 0.10$), and closer to the shroud wall ($x/b = 0.90$) of SVD, ES30 and ES40, it is evident that rotating the diffuser walls causes energy addition to the fluid, thereby raising the dynamic head of the fluid in terms of kinetic energy due to diffusion process. This is well observed in the form of increased stagnation pressure distribution for ES40 as seen in Fig. 14(c), which is discussed later. This addition of energy to the fluid increases with radius ratio as evident from the meridional view plots of absolute velocity distribution for ES40 in Fig. 11 at design flow coefficient, $\Phi = 0.27$. In SVD, the growth of boundary layer is more on the hub side compared to shroud side of the diffuser and the distinct core flow which diffuses as radius ratio increases is clearly visualized.

Also, the magnitude of reduction in absolute velocity is based on the diffusion process efficacy. The effectiveness of the diffusion process is enhanced by the presence of the rotating vaneless diffuser, which is formed by extending the impeller disks alone. Higher the contribution of rotating vaneless diffuser better is the diffusion process as can be seen in static pressure distribution in Fig. 16(a) and Fig. 16(c). However, with the increase in component of rotating vaneless diffuser like in ES40 configuration, there is a deviation from the other shroud extend configurations in terms of magnitude of the values of absolute energy as seen in Fig. 10(c). ES40, which has the highest percentage of rotating part of the vaneless diffuser, the values of absolute velocity show an increasing trend even as the diffusion occurs. This is primarily due to the additional energy imparted to the fluid by the rotating diffuser walls. This is clearly observed in the stagnation pressure distribution as seen in Fig. 14(c) which is discussed later.

The tangential velocity reduces with increase in radius ratios at various flow coefficients for the entire diffuser configurations considered for the present study. Drop in tangential velocity indicates the conversion of kinetic energy into pressure energy due to the diffusion process occurring within the diffuser passage due to through flow which results in this energy transformation. The mass averaged tangential velocity distribution across the width from exit of the impeller to the exit of the diffuser at different radial locations with various flow coefficients is presented in Fig. 12. The reduction in tangential velocity

component from exit of impeller to the exit of diffuser results in rise in the static pressure along the diffuser passage. Tangential velocities of various rotating diffuser configurations (ES10, ES20, ES30 and ES40) are higher than SVD for various flow coefficients. It is observed that the fall in tangential velocities with respect to radius ratio is highest for ES10 compared to SVD. The expected static pressure rise is higher than SVD but much lesser than ES40 and ES30 as seen in Fig. 15 at design flow condition. This is due to the losses that occurs within the through flow passage. With the increasing component of rotating vaneless diffuser, the diffusion process is better in ES40 and ES30 because of the reduced boundary layer thickness on the rotating wall of the diffuser.

With the increasing component of rotating vaneless diffuser for various shrouds extend configurations from ES10 to ES40, the rotating diffuser walls cause further addition of energy to the fluid. This is evident from the Fig. 12 for radius ratios $R = 1.470$ and 1.577 which are the exit locations of the diffuser. ES40, which completely replaces the conventional stationary vaneless diffuser with a forced fully rotating vaneless diffuser, the values of tangential velocities are highest. This is due to comparatively larger work input (i.e., energy level imparted to the fluid) and reduced boundary layer thickness by the rotating walls of the diffuser. Thus, the presence of energy in the form of dynamic head could be converted into an additional static pressure rise in the later stage with a suitable downstream diffusing system. The realized static pressure rise in presence of a suitable casing probably could be higher than the SVD. As seen in the Fig. 13 at $R = 1.470$ and 1.577 , the stagnation pressure distribution for ES40 is highest followed by ES30 for various flow coefficients.

Stagnation pressure reduces with increase in radius ratios at various flow coefficients. Also, as the mass flow rate is increased, the stagnation pressure decreases. The reduction in stagnation pressure shows the magnitude of losses that occurs within the passage of the fluid flow. The stagnation pressure distribution, C_{po} , measured across the width from exit of the impeller to the exit of the diffuser at different radial locations with various flow coefficients is presented in Fig. 13. The drop in stagnation pressure is comparatively larger for SVD as a result of higher losses due to friction that occurs between the through flow and the stationary walls of the vaneless diffuser passage. But in various rotating vaneless diffuser configurations based on shroud extension concept, the shear losses are very much reduced between the through flow and walls of the rotating vaneless diffuser within the passage of the diffuser. Moreover, rotating the walls of the diffuser causes further addition of energy to the fluid. This depends upon the contribution of percentage of the rotating vaneless diffuser component (ES10, ES20, ES30 and ES40) which is revealed clearly in Fig. 13

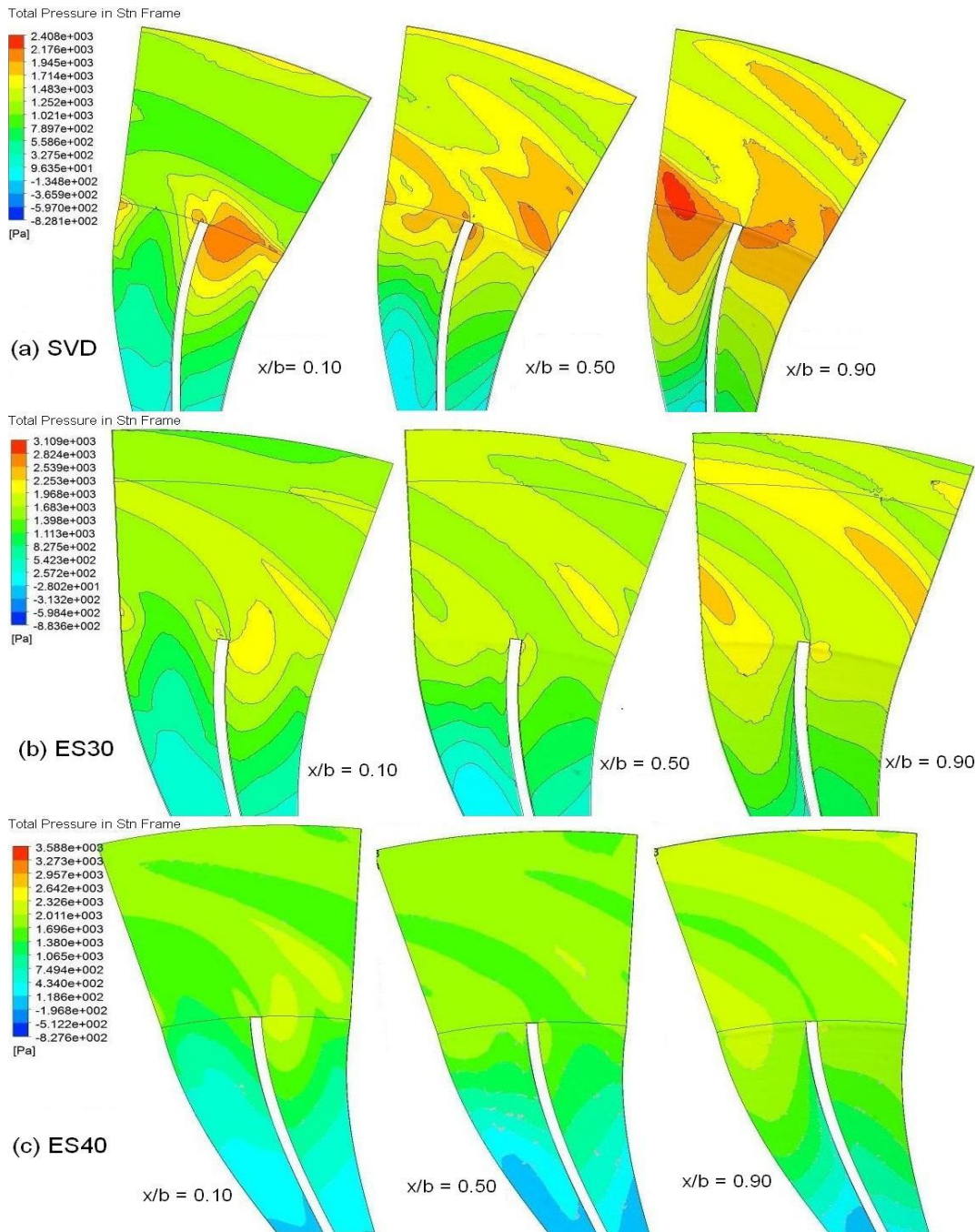


Fig. 14. Contours of stagnation pressure distribution on the axial plane at $x/b = 0.10, 0.50$ and 0.90 for design flow coefficient, $\Phi = 0.27$ for (a) SVD (b) ES30 and (c) ES40 configuration.

and also in the stagnation pressure contours at axial plane from hub to shroud for design flow coefficient, $\Phi = 0.27$ shown in Figs. 14(a), 14(b) and 14(c) for SVD, ES30 and ES40 respectively.

At the mid axial location ($x/b = 0.50$) in comparison with SVD (Fig. 14(a)), the stagnation pressure distribution is found to be nearly uniform at the entry region of fully rotating vaneless diffuser (ES40) as well as at the exit region as seen in Fig. 14(c). Thus, the fully rotating vaneless diffuser tends to smooth out the distorted entry flow profiles

from the impeller exit and thereby increase the performance of the compressor stage of ES40.

As observed from Fig. 13, SVD has the least stagnation pressure coefficient and the value increases in the order of ES10, ES20 and ES30 respectively. It is observed that at diffuser outlet ($R= 1.470$ and 1.577), the stagnation pressure distributions are lower than the diffuser inlet except for fully rotating vaneless diffuser configuration, ES40. In fully rotating vaneless diffuser, due to less shear between the through flow and diffuser walls, the loss is negligible. Further addition of energy to

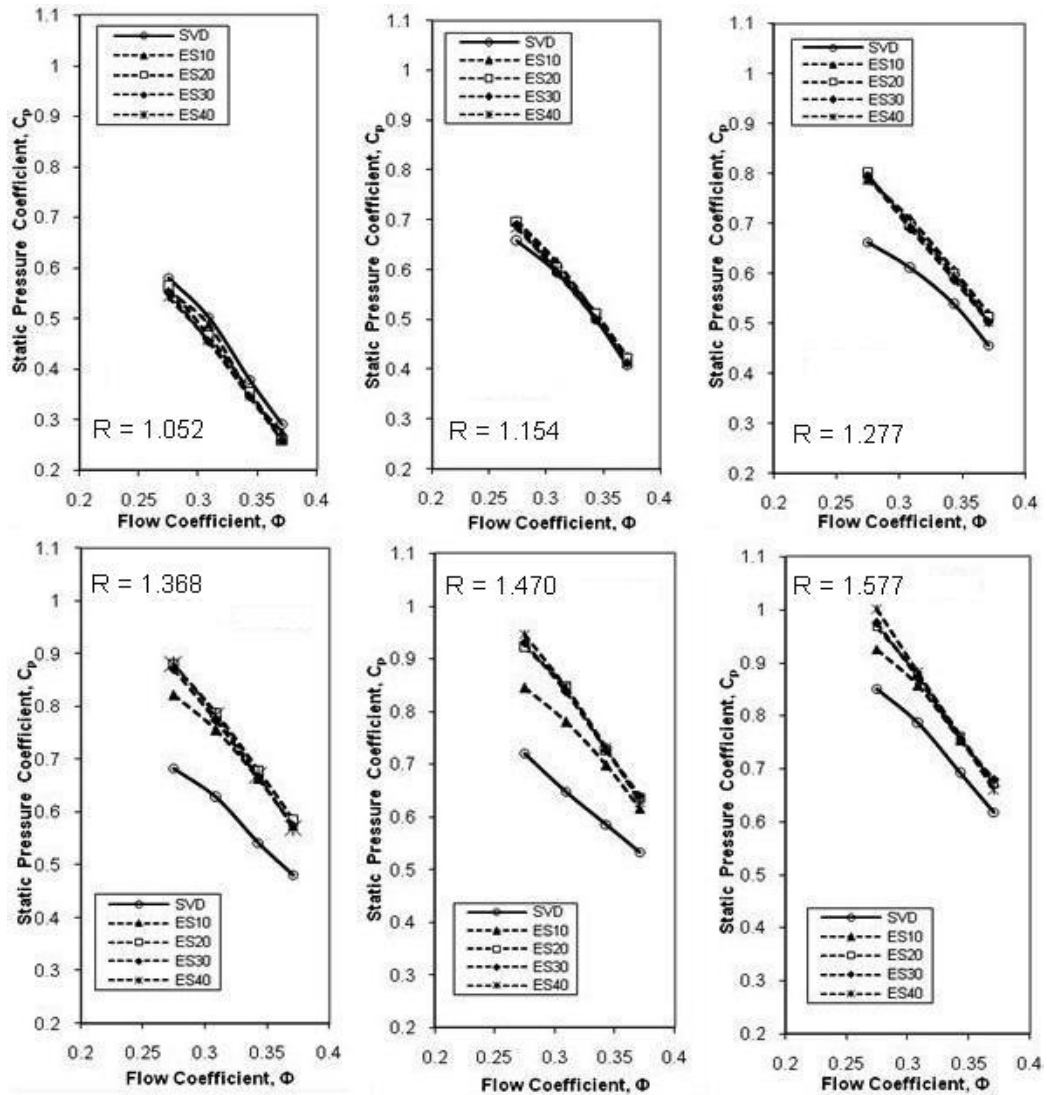


Fig. 15. Variation of static pressure coefficient with flow coefficient for various configurations .

the fluid increases the level of kinetic energy of the fluid, as seen at location $x/b = 0.10$ and $x/b = 0.90$ in Fig. 10(c) and Fig. 14(c), which is available as dynamic head at the diffuser exit (as seen in Fig. 14(c)). With a suitable downstream diffusing system, this could be further converted into an additional static pressure rise.

Generally, due to diffusion of flow, the static pressure increases with increase in radius ratios. The static pressure distribution, C_p , observed across the width from exit of the impeller to the exit of the diffuser at different radial locations with various flow coefficients is presented in Fig. 15. As the mass flow rate is decreased, the extent of static pressure rise increases at any section, similar to the stagnation pressure distribution. At diffuser inlet ($R = 1.052$), the static pressure distribution for various shroud extend configurations is slightly lesser than SVD for design and above design flow coefficients. At $R = 1.470$ and 1.577 , the static pressure rise and distribution of various shroud extend configurations are higher than SVD. The static pressure

distributions for various shroud extensions are in similar range at off-design flow conditions. ES40 offers the highest rise in static pressure by around 9.84% than SVD (as also seen in Fig. 16(a) and Fig. 16(c)) at design flow coefficient $\Phi = 0.27$ followed by ES30.

The fully rotating vaneless diffuser configuration (ES40) which gives a higher rise in static pressure compared to SVD is also reflected with highest static pressure recovery coefficient at the diffuser exit (as seen in Fig. 7(a)). The static pressure contours at axial plane from hub to shroud at $x/b = 0.10$ (closer to the hub wall), 0.50 (mid axial location) and 0.90 (closer to the shroud wall) for design condition, $\Phi = 0.27$, are shown in Figs. 16(a), 16(b) and 16(c) for SVD, ES30 and ES40 respectively. In typical rotating vaneless diffusers, the walls of the vaneless diffusers (i.e., extended impeller disks) rotate. The particles of fluid that are located closer to the wall of the vaneless diffuser also rotate with equivalent angular velocity and as the position is moved away from the rotating

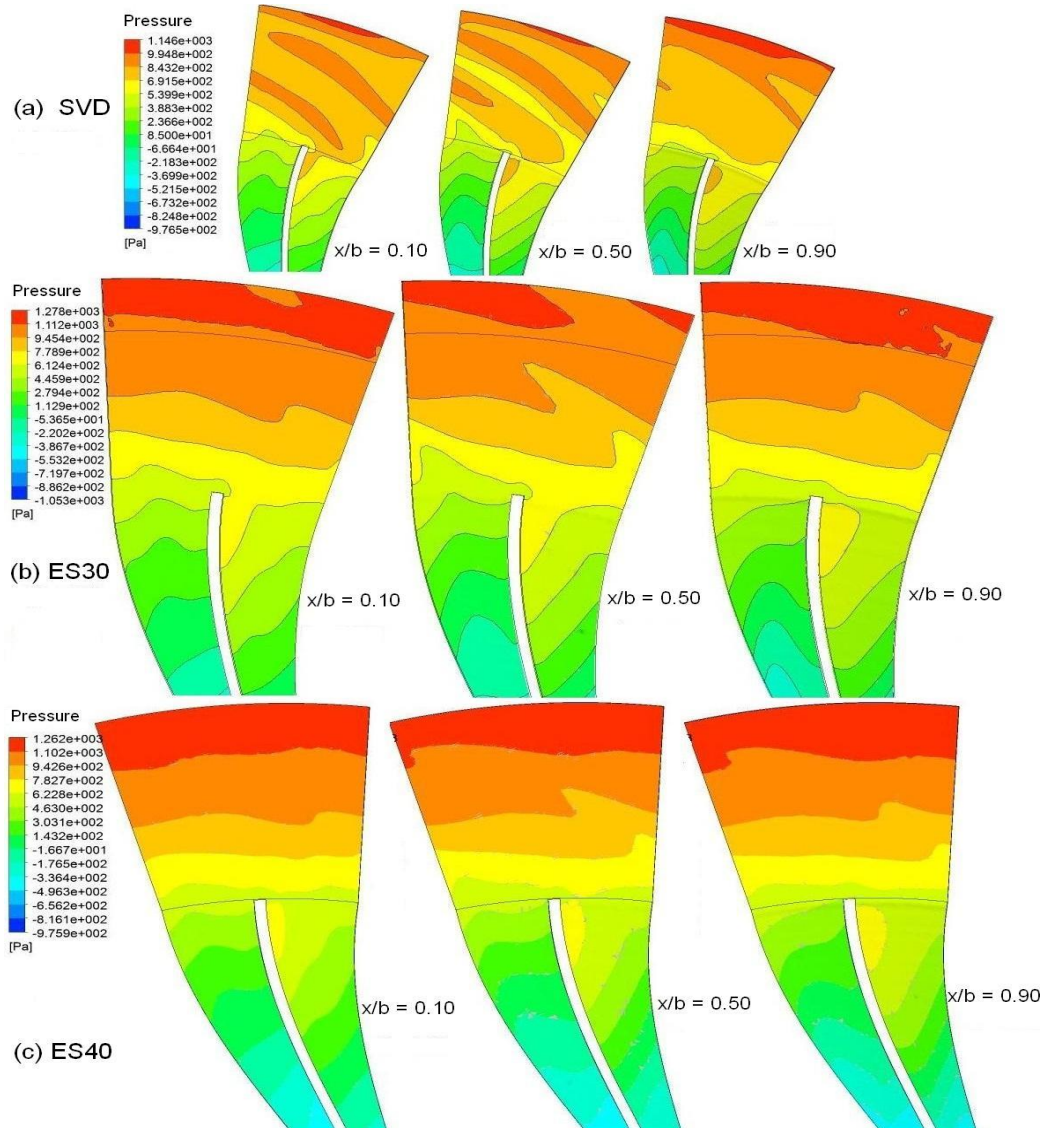


Fig. 16. Contours of static pressure distribution on the axial plane for design flow coefficient, $\Phi = 0.27$.

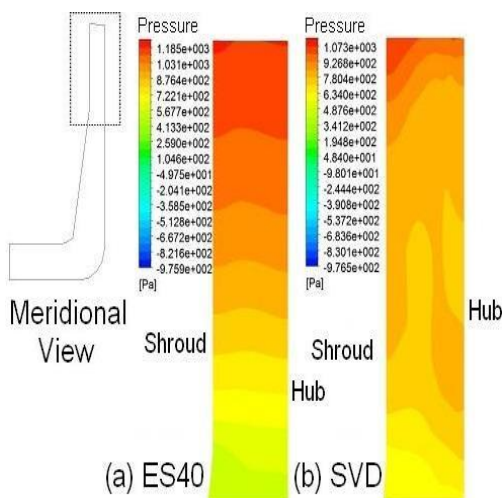


Fig. 17. Meridional view plots of static pressure distribution for ES40 and SVD at $\Phi = 0.27$.

diffuser wall, the angular velocity decreases. As walls of the diffuser rotate in the rotating vaneless diffuser, additional energy transfer takes place to the fluid (as seen in Fig. 11). This transforms into static pressure rise gain due to diffusion as the flow goes to next level of radius ratios. This is reflected with fully rotating vaneless diffuser, ES40 (as seen in Fig. 17) offering higher static pressure rise among the shroud extension configurations followed by ES30 which is mainly due to the higher percentage of rotating part of the vaneless diffuser compared to other extended shroud configurations. This establishes clearly that diffusion process is better in shroud extension configurations in general and in the fully rotating vaneless diffuser based on shroud extension concept (ES40), the diffusion rate is higher compared to conventional stationary vaneless diffuser (SVD) of equivalent diffuser diameter ratio of 1.40.

6. CONCLUSION

A numerical study has been carried out to understand the effect of forced rotating vaneless diffuser created by extending the impeller disks alone (i.e., hub and shroud portion of the shrouded type impeller) on the performance characteristics and flow parameters of a low-pressure ratio centrifugal compressor stage under different flow coefficients. The conclusions mentioned below are drawn from this present computational investigation.

ES10 has the highest efficiency, whereas ES40 has the lowest efficiency. The efficiency of ES40 is lesser compared to SVD by around 5.40% to 3.43% at design as well as above off-design flow conditions. Almost equal efficiencies are obtained for SVD and ES30. ES40 records the highest stage energy coefficient followed by ES30 compared to SVD. The static pressure recovery for ES40 is higher at design flow coefficient, $\Phi = 0.27$ and is nearly equivalent to that of ES30 at above design flow conditions. Static pressure rise in ES40 is higher than SVD at various flow rates. At design flow condition $\Phi = 0.27$, it is higher by around 9.84%. A marginally higher rise in static pressure is achieved by ES40 at design flow condition in comparison with ES30 configuration. Also, the rise in static pressure of ES40 is nearly equivalent to that of ES30 at off-design flow conditions.

The stagnation pressure loss coefficient of ES40 reduced drastically compared to SVD. By comparing the contours of stagnation pressure distribution and absolute velocity distribution closer to the hub and shroud walls ($x/b = 0.10$ and $x/b = 0.90$) of ES40 and SVD, it is observed that an additional energy is added to the fluid by the rotating walls of the vaneless diffuser. This adds up the kinetic energy level of the fluid which due to diffusion results in gain of the static pressure rise. Also, the shorter flow path with higher relative flow angle causes reduced losses due to friction in the rotating vaneless diffuser by shroud extend configuration in comparison with the conventional stationary vaneless diffuser. There is a net increase in stagnation pressure distribution at the exit of diffuser due to rotating vaneless diffuser. The fully rotating vaneless diffuser (ES40) also tends to smooth out the distorted entry flow profiles from impeller exit, thereby increasing the performance of the centrifugal compressor stage. This signifies that the diffusion process is enhanced in the low-pressure ratio centrifugal compressor stage with a fully rotating vaneless diffuser (ES40) which is achieved without any major design modification and constructional arrangement of a centrifugal compressor.

REFERENCES

- Aboujaib, M. M., L. Bayeul and C. Annie (1998). Computational fluid dynamics'98. In *Proceed-*

ings of the 4th European Computational Fluid Dynamics Conference, Athens, Greece. 1, 279-284.

Cheng, X. U. and R. S. Amano (2012). Empirical design considerations for industrial centrifugal compressors. *International Journal of Rotating Machinery* 2012, Article ID 184061, 15 Pages.

Erwin, J. R. and N. G. Vitale (1969). The Radial Outflow Compressor. In *Proceedings of the ASME Gas Turbine Conference*.

Govardhan, M. and S. Seralathan (2011). Effect of forced rotating vaneless diffusers on centrifugal compressor stage performance. *Journal of Engineering Science and Technology* 6(5), 558-574.

Govardhan, M., B. S. N. Moorthy and G. Gopalakrishnan (1978). A preliminary report on the rotating vaneless diffuser for a centrifugal impeller. In *Proceedings of the 1st International Conference on Centrifugal Compressor*, IITM, Chennai, India.

James, M. S. (2011). Range vs efficiency. In *Proceedings of the 40th Turbomachinery Symposium*, Houston, Texas, USA 153-169.

Northern Research and Engineering Corporation (1976). Improvements in surge margin and diffuser performance: design, test and analysis report for task IV stage configurations '50 degree backslop shrouded impeller series, *Report 1230-4*.

Novak, J. (1907). Smooth diffusers in centrifugal pumps (in German). *Z. Ges. Turbinenwesen* 24.

Sapiro, L. (1983). Effect of impeller-extended shrouds on centrifugal compressor performance as a function of specific speed. *ASME Journal of Engineering for Power* 105, 457-465.

Seralathan, S. and D. G. Roy Chowdhury (2013). Modification of centrifugal impeller and effect of impeller extended shrouds on centrifugal compressor performance. *Procedia Engineering* 64, 1119-1128.

Seralathan, S. and D. G. Roy Chowdhury (2014). Performance enhancement of the centrifugal compressor stage with a rotating vaneless diffuser – a numerical study. In *Proceedings of the ASME 2014 Gas Turbine India Conference*, New Delhi, India, ASME Paper.

Seralathan, S., D. G. Roy Chowdhury and A. K. Jaswal (2014). Enhancement of flow diffusion in a centrifugal compressor stage with backward curved impeller by shroud extension a numerical study. *Advanced Materials Research* 984-985, 1102-1107.

Yasutoshi, Senoo (2005). Researches on fluid dynamics of centrifugal compressors. *Proc. Japan Acad., Ser. B* 81, 77-85.